Article

Effect of Post-Drawing Thermal Treatment on the Mechanical Behavior of Solid-State Drawn Poly(lactic acid) (PLA) Filaments

Martín Butto [1,2], **María Lluisa Maspoch [3]** and **Celina Bernal [1,2,*]**

1   Universidad de Buenos Aires, Facultad de Ingeniería, Ciudad Autónoma de Buenos Aires C1063ACV, Argentina; mbutto@fi.uba.ar
2   CONICET-Universidad de Buenos Aires, Instituto de Tecnología en Polímeros y Nanotecnología (ITPN), Av. Las Heras 2214, Ciudad Autónoma de Buenos Aires C1127AAR, Argentina
3   ePLASCOM Research Group, Centre Català del Plàstic (CCP), Universitat Politècnica de Catalunya Barcelona Tech (EEBE-UPC), Av. Eduard Maristany, 14, 08019 Barcelona, Spain; maria.lluisa.maspoch@upc.edu
*   Correspondence: cbernal@fi.uba.ar

Abstract: In this work, two commercial extruded filaments for 3D printing obtained from different NatureWorks PLA resins (Ingeo™ Biopolymer 3D850 and Ingeo™ Biopolymer 4043D) were solid-state drawn at varying temperatures and subsequently heat treated by annealing. The aim was to analyze the effect of post-processing of industrial fibers (solid-state drawing and annealing treatment) with varied composition (PLA grades with different contents of D-isomer) on the mechanical performance and thermal stability of the obtained PLA fibers. Morphological, thermal, and mechanical characterizations were performed for the undrawn filaments and drawn fibers, both before and after heat treatment. Drawn fibers presented a fibrillar core–shell structure, and their mechanical properties were greatly improved with respect to undrawn filaments in accordance with their higher crystallinity. The resin with the higher content of D-isomer (4043D) resulted in lower crystallinities with a subsequent decrease in mechanical properties. After heat treatment, drawn fibers exhibited completely different behaviors depending on the PLA resin, with 3D850 fibers being much more stable than 4043D fibers, which underwent molecular orientation upon drawing rather than crystallization. The solid-state drawn fibers obtained herein are comparable to commercial fibers in terms of mechanical properties.

Keywords: poly(lactic acid); solid state drawing; polymeric filaments; thermal treatment; mechanical behavior

1. Introduction

Poly(lactic acid) (PLA) is a compostable polymer obtained from renewable sources. It belongs to the family of aliphatic polyesters derived from the simplest of the α-hydroxy acids, namely lactic acid. This molecule can exist as two optically active enantiomers, L-and D-lactic acid. After polymerization, PLA has stereoisomers such as poly(L-lactic acid) (PLLA), poly(D-lactic acid) (PDLA), and poly(DL-lactic acid) (PDLLA). The isomer proportion leads to different material properties, allowing the production of a wide spectrum of PLA polymers [1]. PLA can be processed in most polymer processing equipment and can also be formed into transparent films, fibers, or injection molded into blow-moldable preforms for bottles [2]. It has good optical, physical, mechanical, and barrier properties compared to existing petroleum-based thermoplastics. Mechanically, unoriented PLA is quite brittle but has a good combination of strength and stiffness, while the oriented polymer provides better performance [3].

Quite extensive research has been carried out on the crystallization process of PLA and the effects of molecular weight, D-isomer content, and thermal history. The optimal temperature to crystallize PLA is very sensitive to the D-isomer content [4] and molecular

weight [5], and it can crystallize in different polymorphs depending on the processing conditions [6].

The influence of the processing conditions on the morphology and thermal and mechanical behavior of melt-spun PLA filaments has been investigated in the literature [7]. It was found that the melt draw ratio (ratio of extrusion speed and take-up speed during spinning), solid-state draw ratio, and drawing temperature were the major determining factors of the PLA fibers mechanical properties. Their orientation and crystallinity were observed to increase with the solid-state draw ratio, which was related to the melt draw ratio. To obtain highly oriented and crystalline PLA fibers that exhibit high tenacity, a higher solid-state draw ratio and a lower melt draw ratio are required.

To promote crystallization and improve its properties, PLA can be annealed after processing [5,8,9]. Some authors have studied the influence of annealing time and temperature on fully amorphous samples of PLLA of different molecular weights. They have found that the process is fastest when higher temperatures are employed, and most of the crystallization process happens in the first 20 min. Nevertheless, severe degradation takes place during the annealing process, even under a nitrogen atmosphere, and consequently, treatment times should be as short as possible [5]. The annealing process has also been studied in samples where the α' crystalline form was already present. In this case, both annealing time and temperature have significant effects on the α' to α transition, which is faster when higher temperatures are employed. Relevant changes were seen after heat treating α' crystalline form at sufficiently high temperatures for 10 min [6].

It is also worth noting that synthetic fibers find a huge number of applications in different sectors, such as medicine, sports goods, textiles, etc. Among them, polymeric fibers such as those produced from polyamides, polyester, and polypropylene are the most used for textile applications [10]. Over recent decades, there has been a growing interest in both academia and industry in the development of biodegradable fibers, with those obtained from PLA being the most preferred ones [11].

Commercial PLA fibers are generally produced by a two-stage process: melt extrusion, followed by solid-state drawing. In this way, stiff, strong, and highly oriented fibers can be obtained [12]. Since many processes in the textile industry [13] and in the manufacture of composite materials are performed at high temperatures [14], the study of the dimensional stability and properties of fibers after heat treatments is of significant importance [15]. Some works focused on the effect of thermal treatments on solid-state filaments drawn under different mild conditions. Thermal and mechanical properties were also analyzed both before and after a stabilization treatment was employed, with thermal shrinkage measured under both wet and dry conditions and under taut and free conditions, respectively [16,17].

The aim of this work was to analyze the effect of post-processing of industrial fibers (solid-state drawing and subsequent thermal treatment of annealing) with varied composition (PLA grades) on the mechanical performance and thermal stability of the PLA fibers. Two commercial extruded filaments for 3D printing obtained from different PLA resins were solid-state drawn. The effect of the drawing temperature and the subsequent annealing applied to PLA fibers with different D-isomer contents was analyzed. The obtained fibers were investigated through morphological, thermal, and mechanical characterizations. These fibers have potential applications as reinforcement in biodegradable, self-reinforced PLA composites; hence, their mechanical properties and thermal stability are of major importance.

2. Materials and Methods

2.1. Materials

Two different commercial extruded 1.75 mm filaments for 3D printing manufactured by Kaviflex S.R.L. from NatureWorks LLC (Plymouth, MN, United States) resins were used in this work. Ingeo™ Biopolymer 4043D is a multi-purpose extrusion grade recommended for biaxially oriented films and 3D printing filaments. On the other hand, Ingeo™ Biopoly-

mer 3D850 is a commercial grade specifically developed for 3D printing with an improved crystallization rate. The characteristics of both resins are presented in Table 1.

Table 1. Characteristics of the studied materials.

Resin	Melt Flow Index MFI (210 °C/2.16 kg)	Density δ (g/cm³)	D-Isomer Content (wt.%)
3D850	7–9 [9]	1.24 [9]	0.5 [18]
4043D	7–9 [19]	1.24 [19]	2–5 [20,21]

Commercial fibers of PLA kindly provided by Noyfil (Radici Group. Bergamo, Italy) S.p.A (144 continuous filaments, each with a diameter of 20.5 ± 0.8 μm [22]) were also used in this work for comparison purposes.

2.2. Filament Drawing

The commercial filaments were solid-state drawn in a fit-for-purpose in-lab machine (Figure 1), similar to the one described in [23], after storage under vacuum at RT, and hence, no significant effect of water molecules on plasticization or on the rate of hydrolysis was expected [24]. The filament was preheated in a 50 mm in diameter and 1 m long tubular furnace set to 65 °C and then drawn in another similar furnace set at 170 °C and 180 °C for the 3D850 resin and at 140 °C, 150 °C, and 160 °C for the 4043D resin. At each end of the drawing furnace, there are two pulley trains driven by three-phase asynchronous motors controlled by independent frequency converters in an open-loop control system. A former version of this machine, with a different furnace temperature profile and filament feeding mechanism, has already been described in a previous paper [23].
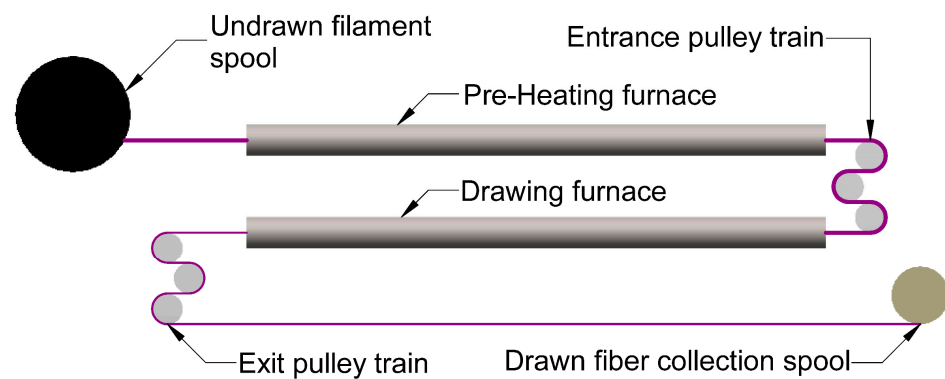
Figure 1. Solid-state drawing machine schematics.

Speeds were varied until a stable operating condition was reached. Due to motor limitations, only an idle 29 mm/s entrance speed and 204 mm/s exit speed resulted in a stable operating condition. Actual processing speeds depend on the machine's load state. High-speed recordings taken with a Samsung Galaxy S10 phone camera at 120 fps show speed changes of up to 10% in both entrance and exit pulley trains when compared to idle speeds. The filament draw ratio (*DR*) can be defined as the quotient between the entrance and exit speeds of the drawing furnace, or analogously as the relationship between the filaments initial and final cross-sectional areas.

$$DR = \frac{V_{exit}}{V_{entrance}} = \frac{A_{initial}}{A_{final}} = \left(\frac{D_{initial}}{D_{final}} \right)^2,$$ (1)

The tubular drawing furnace has a parabolic temperature profile (Figure 2): the furnace set temperature (FST) is reached in the middle section while it decreases on both sides. The filament's drawing concentrates in a small region near the machine's center, where

the furnace temperature reaches a maximum. The filament progressively heats up until it yields and deformation begins. In the deformation process, molecules become axially aligned, and the material's elongational viscosity decreases rapidly due to strain thinning. This leads to fast deformation and diameter reduction, which, in turn, increase the stress level and further induce deformation in a small region, forming a "neck". When high molecular orientation is reached, freedom of motion is lost due to crystal formation. The partially crystalline material behaves like rubber and shows a strain-hardening behavior that arrests any further deformation, as described in [25]. A cross-section profile measured from a cooled-down filament is also shown in Figure 2.
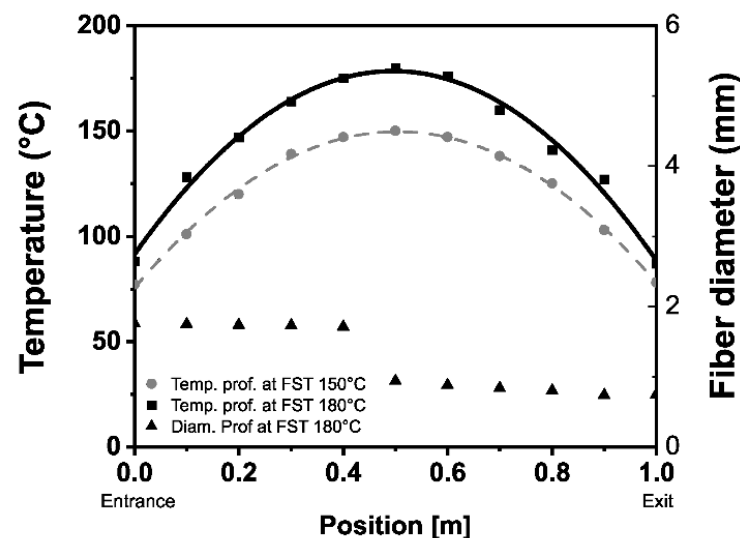

Figure 2. Temperature and section profile inside the drawing furnace at different set temperatures.

Filament temperatures were controlled at the exit of the furnace using a Testo 882 infrared camera (320×240 pixels resolution, 0.2 m focus distance, 1.7 mrad IFOV, and ± 2 °C or 2% accuracy). When the FST was 180 °C, the filament at the exit was at 100 °C, thus suggesting that it did not reach the material's melting temperature during the drawing process.

2.3. Post-Drawing Heat Treatment

To investigate the filaments' thermal stability and the effect of annealing, unrestricted solid-state drawn filaments (310 ± 2 mm long) were subjected to a heat treatment after storage under vacuum at RT. Both resins used in this work were annealed at 120 °C, since it is in the recommended range for Ingeo™ Biopolymer 3D850 (NatureWorks LLC, Plymouth, MN, USA) resin (post-processing annealing treatment in the range of 80–130 °C to promote crystallization of 3D printed parts [9]) and it is very close to the cold-crystallization peak temperature of the Ingeo™ Biopolymer 4043D resin, as it will be shown in Section 3.2. In the 4043D resin, the presence of D-isomer limits the maximum crystallinity attainable when crystallized under stress and hinders the quiescent crystallization process, but given sufficient time and temperature, the material can still crystallize [3]. All samples were annealed for 20 min to limit material degradation since it has been shown in the literature that most of the cold crystallization process takes place during this period and treatment times should be as short as possible, as already mentioned [5].

2.4. Filaments Characterization

Drawn filaments were axially cut to extract the middle section and observe the cores' structure using bright field microscopy. Two cuts were performed using a sharp blade to remove the fiber's outer surface so that it did not interfere with the observations and white light could go through the sample. Additionally, fiber surfaces were sputter coated with a thin layer of gold before scanning electron microscopy (SEM) observation in a Quanta 200 microscope (FEI, Hillsboro, OR, USA) using a voltage of 5 kV.

Filaments diameters were measured at least four times at different sections using a digital comparator (Asimeto, Mooresville, NC, USA, Series 450, accuracy ±0.01 mm), and their lengths before and after heat treatment were measured with a metallic ruler.

Molecular weight was determined by size exclusion chromatography (SEC) on a system built with a Waters 515 HPLC pump and a Waters model 2414 refractive index detector, equipped with four PLGel® columns with 10 μm bead size and 500, 104, 105, and 106 Å porosity, respectively. Solutions of PLA in tetrahydrofuran with concentrations between 1 and 2 mg/mL were prepared at room temperature, and measurements were made from 200 μL samples injected at a rate of 1 mL/min. Polystyrene (PS) standards were used for calibration. Molecular mass distributions and average molecular weights were calculated using the corresponding Mark–Houwink calibration constants (KPS = 1.28×10^{-4} dL/g, KPLA = 1.74×10^{-4} dL/g, αPS = 0.695 and αPLA = 0.740).

Differential scanning calorimetry (DSC) analysis was performed using a Shimadzu DSC-60. A single heating scan was analyzed to evaluate the processing effects using a heating rate of 10 °C/min from room temperature to 200 °C under a continuous 30 mL/min flow of nitrogen. The crystallinity percentage X_c was calculated according to Equation (2) relating the measured melting enthalpy ΔH_m, the cold crystallization enthalpy ΔH_{cc} and the melting enthalpy for 100% crystalline PLA ΔH_{m0} (93.6 J/g [4]).

$$X_c = \frac{\Delta H_m - \Delta H_{cc}}{\Delta H_{m0}} \tag{2}$$

Uniaxial tensile tests were carried out in an Instron 5985 dynamometer at room temperature following ISO 527-1:2019 standard [26] recommendations. The material was stored at room temperature for at least a week prior to mechanical testing to allow for proper physical aging [27]. Four or more samples from each condition were tested using a gripping distance of 30 mm at a 10 mm/min displacement speed. Tensile apparent modulus, yield strength, and stress and strain at break were determined from the stress–strain curves obtained.

3. Results and Discussion

*3.1. Morphological and Dimensional Analysis*

Both undrawn filaments (3D850 and 4043D) are transparent and colorless. After drawing, a severe reduction of the fiber's diameter was observed, and they became white and opaque. After heat treatment, the undrawn filaments turned opaque, which can be attributed to crystal formation [28], while the drawn filaments remained unchanged.

Drawn fibers obtained from 3D850 resin have a very thin white skin and a transparent core that becomes slightly opaque near the center (Figure 3). On the other hand, fibers drawn from 4043D resin had a similar structure to those made from 3D850 resin, but they displayed a well-defined second opaque core at the center (Figure 4). The change in color on the fiber's skin has been attributed in the literature to the formation of surface crazes as a result of the high stresses developed upon drawing [29]. Likewise, the opaque zones on the fiber core could be due to crazing or the formation of micro-voids during crystal formation caused by over-drawing, as reported in [17,19]. Since fibers were heated from the outside, the core was expected to be colder. The conditions on the core might have limited solid-state drawing, and a greater number of micro-voids could have formed. No significant morphological differences were observed among fibers drawn at different temperatures, and in all cases, microfibrils detached from the cut surfaces, which were better appreciated on the lateral views of Figures 3 and 4.
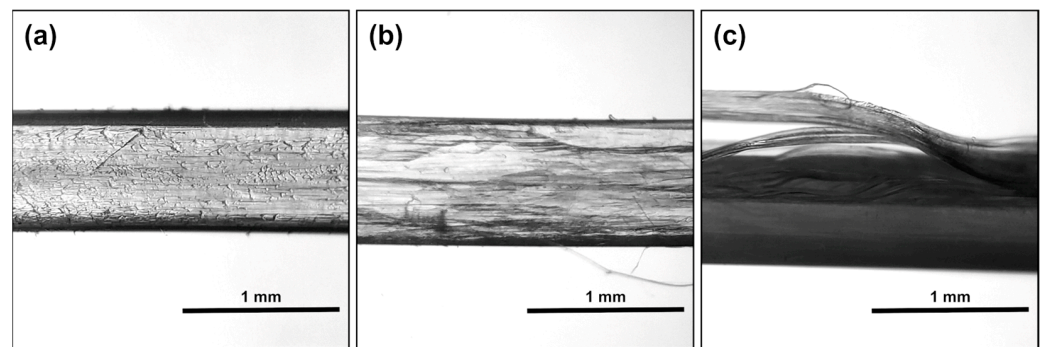
Figure 3. Core of a 3D850 fiber drawn at FST 180 °C (**a**) before heat treatment, (**b**) after heat treatment, and (**c**) lateral view of the section of the fiber before heat treatment.
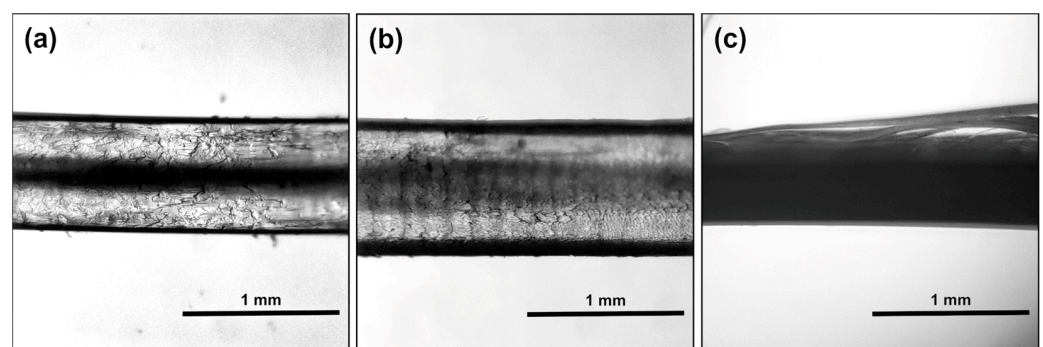

Figure 4. Core of a 4043D fiber drawn at FST 160 °C (**a**) before heat treatment, (**b**) after heat treatment, and (**c**) lateral view of the section of the fiber before heat treatment.

While handling the drawn fibers, microfibrils were pulled out from the surface, and a structure resembling a spider's web was generated. A closer inspection using SEM of the microfibrils detached from the surface showed that they were composed of even smaller structures aligned in the fiber's direction, as shown in Figure 5 for a 3D850 fiber drawn at a FST of 170 °C as an example. A highly fibrillar morphology of PLA fibers has already been reported in the literature [29]. It develops from the chain alignment in the direction of the orienting force upon drawing and has been related to the morphology observed in PET, where each microfibril is composed of alternating lamellae of crystalline and amorphous regions and where interfibrillar domains consist of aligned but noncrystalline molecules referred to as interfibrillar tie molecules. These molecules are unrestricted by the microfibrils and are able to freely deform. If the area of interfibrillar tie molecules is large enough, the microfibrils will slip past each other as a result of the weak interactions between them [29], as observed on the surface of the drawn PLA filaments investigated in this work.

After heat treatment, all fibers still displayed the same core–shell structures they had exhibited before (Figures 3 and 4). In addition, dark and light bands perpendicular to the fiber axis were observed in the treated 4043D fiber, indicating areas where crazing was occurring [29]. Microfibrils were still observed to detach from the 3D850 cut surfaces after heat treatment, while no microfibrils were found on the cuts of the 4043D fibers.

It has been reported in the literature that annealing induces changes in the lamellar and fibrillar structures of PET fibers, including the thickening and broadening of crystalline lamellae, the decrease in lamellar inclination, and the increase in interlamellar amorphous thickness. Also, amorphous chain coiling and loss of orientation after treatment occur. If the annealing temperature is high enough, chain mobility will be significant, and crystallization is possible at either end of the fibrils, which grow longer and become more oriented along the fiber axis. It is also possible that smaller fibrils link together through molecular movement and crystallization [30]. Similar to what happens in PET fibers after annealing,

the fibrillar structure of 4043D fibers investigated here would have experienced significant changes during treatment, which would have been higher than those of 3D850 fibers due to their relatively higher annealing temperature.
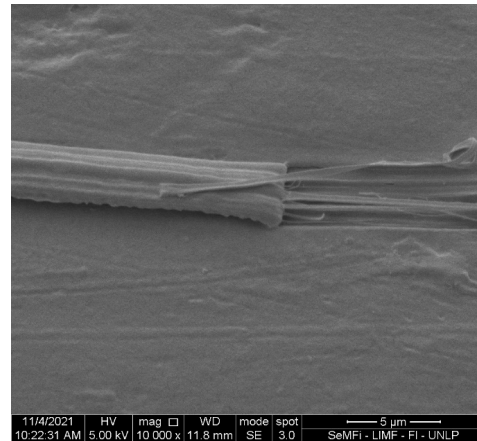
Figure 5. SEM micrograph of a microfibril partially detached from a 3D850 fiber drawn at a FST of 170 °C.

Average diameters and their errors are shown in Table 2. Drawn fibers made from the 3D850 resin showed no significant differences in their dimensions when the processing temperature was changed. Conversely, the diameters of fibers drawn from 4043D resin were dependent on the processing temperature. Even though the machine´s setup was not varied, the force required to draw the filaments changed with temperature, which in turn affected the speed of the machine's asynchronous motors and consequently the applied draw ratio. After heat treatment, all samples increased their diameter and became shorter, except the undrawn 3D850 filament, which remained unchanged. No significant volume changes were observed since, in all cases, they were within the experimental error.

Table 2. Fiber average diameters and their errors, mean draw ratio, and change in length after heat treatment (ΔL) for all studied conditions.

Resin	Condition	*DR*	*ΔL*	Fiber Diameter	
				Not Treated (mm)	Heat Treated (mm)
3D850	Undrawn	-	1%	1.74 ± 0.02	1.72 ± 0.01
	FST 170 °C	5.5	−12%	0.74 ± 0.01	0.78 ± 0.02
	FST 180 °C	5.4	−10%	0.75 ± 0.01	0.78 ± 0.01
4043D	Undrawn	-	−8%	1.73 ± 0.03	1.79 ± 0.01
	FST 140 °C	5.6	−36%	0.73 ± 0.02	0.93 ± 0.03
	FST 150 °C	5.3	−35%	0.75 ± 0.01	0.86 ± 0.03
	FST 160 °C	5.9	−35%	0.71 ± 0.01	0.88 ± 0.03

It is important to note that the change in length after heat treatment (ΔL) of the 4043D filament was found to be much more significant than that of the 3D850 filament under all conditions. This can be attributed to the lower ability of that resin to crystallize due to its higher content of D-isomer. Hence, in contrast to what happens in the 3D850 filaments, molecular orientation in the 4043D filaments can mostly occur upon drawing rather than crystal formation.

In addition, average molecular weights in number (*Mn*) and weight (*Mw*) and the corresponding polydispersity index (*PDI*) values were measured before and after the solid-state drawing process to assess if any degradation took place during processing (Table 3). *Mn* and *Mw* of the 3D850 resin decreased after drawing an average of 8.5% and 4.5%,

respectively, showing similar results to those reported by other authors [31]. On the other hand, 4043D resin did not show a significant change in molecular weights after processing.

Table 3. Average molecular weights measured before and after solid-state drawing.

Resin	Condition	M_n (kg/mol)	M_w (kg/mol)	PDI (Mw/Mn)
3D850	Undrawn	69.7 ± 1.9	113.4 ± 2.7	1.6 ± 0.1
	Drawn	63.8 ± 1.2	108.4 ± 2.7	1.7 ± 0.1
4043D	Undrawn	74.8 ± 1.6	122.4 ± 1.8	1.6 ± 0.1
	Drawn	75.5 ± 2.3	119.4 ± 1.5	1.6 ± 0.1

3.2. Thermal Behavior

DSC heating thermograms for the original and drawn filaments both before and after heat treatment are presented in Figure 6. Both original filaments before treatment exhibited a glass transition, a cold crystallization peak, and a melting peak. The cold crystallization peak of the 3D850 resin was well defined and at quite low temperatures, whereas in the 4043D resin it was very broad, small, and at high temperatures due to the relatively high content of D-isomer, which restricted the material's ability to crystalize as already mentioned. A second exothermic peak was also observed on the undrawn 3D850 filament, which has been associated in the literature with the reorganization of the α′ crystalline structure into the α form immediately before melting starts [32]. As expected, the 4043D resin melted at lower temperatures and achieved a lower crystallinity, which is consistent with the higher D-isomer content and explains why this resin had to be solid-state drawn at lower temperatures. The average values of the glass transition onset temperature (T_g), cold crystallization (T_{cc1}), melting peak temperatures (T_m), and crystallinity (X_c) are presented in Table 4.
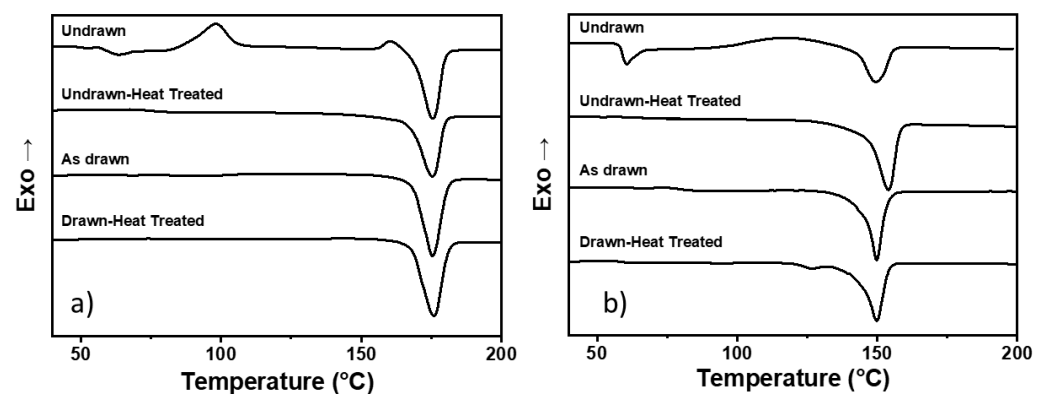
Figure 6. Heating thermograms obtained by DSC for original and drawn filaments before and after heat treatment: (**a**) 3D850 undrawn filament and fiber drawn at a FST of 180 °C and (**b**) 4034D undrawn filament and fiber drawn at 160 °C.

Table 4. Thermal parameters of the undrawn 3D850 and 4043D filaments both before and after heat treatment.

Resin	Condition	T_g (°C)	T_{cc1} (°C)	T_{exo} * (°C)	T_m (°C)	X_c (%)
3D850	Undrawn	57.1 ± 0.8	98.2 ± 0.8	160.2 ± 0.3	175.4 ± 0.2	18.7 ± 2.7
	Undrawn-HT	70.6 ± 1.1	-	-	175.5 ± 0.1	51.3 ± 0.9
4043D	Undrawn	57.5 ± 0.4	117.5 ± 0.3	-	149.6 ± 0.2	4.2 ± 2.0
	Undrawn-HT	55.6 ± 0.6	-	-	153.7 ± 0.3	41.8 ± 1.1

* Peak temperature of the second exothermic peak.

An endothermic peak attributed to physical aging was also present in the region where the glass transition occurred for both untreated filaments. The amorphous regions of the polymer are in a metastable state when rapidly cooled after processing, having an excess of enthalpy, entropy, and free volume that act as a driving force for the aging process. Given sufficient time, these regions tend to reorganize into ordered domains that need more energy to undergo the glass transition, which manifests as the endothermic peak seen on the thermograms [33].

After heat treating the undrawn filaments, the cold crystallization peaks were no longer present, and the glass transition became less pronounced. During heat treatment, crystals were formed, and they hindered molecular movement in the amorphous phase, which resulted in the fainter glass transition seen on the thermograms in Figure 6 and turned the material opaque, as pointed out in Section 3.1. After the heat treatment, the peak associated with the α'-α transformation of the 3D850 resin also disappeared, implying that during heat treatment the material had enough time to fully develop the α crystalline structure. The glass transition onset temperature, melting peak temperature, and crystallinity values after the heat treatment are also reported in Table 4.

A great increase in crystallinity was seen after heat treating both undrawn filaments, but, as expected, the resin with more D-isomer content reached lower values since the presence of the second isomer hindered crystallization. The peak melting temperature of the 3D850 undrawn filament was not affected by the heat treatment, but in the 4043D undrawn filament, it increased after annealing. Undrawn, untreated 4043D fiber was almost completely amorphous and crystallized during the DSC scans. Since it was heated at high speeds, there was insufficient time for the α crystalline form to fully develop, and instead, the distorted α' form was generated. When the crystallization process was carried out in an oven, the sample remained at high temperatures for longer without melting, enabling the formation of bigger and more perfect crystallites that are expected to melt at higher temperatures [8]. Finally, there were also significant differences in the effect of annealing on the glass transition temperatures of both materials. While the undrawn 4043D filament presented similar T_g values irrespective of the heat treatment, in the 3D850 filament, the annealing led to an increase in T_g. This could be attributed to the more restricted movement of the amorphous phase in this case.

The solid-state drawn fibers presented a much higher crystallinity than the undrawn filaments. High molecular orientation is derived from drawing, which subsequently leads to crystal formation. These fibers showed a similar thermal behavior to the undrawn, heat-treated samples. The glass transition became fainter and took place at higher temperatures, and no cold crystallization peaks were observed on the thermograms. All drawn fibers of both resins presented their melting peaks at the same temperature as the undrawn, untreated filaments. This result suggests that the crystals formed in the 4043D resin were of the distorted α' form. In addition, there were no significant differences in the melting temperatures or crystallinity of fibers of the same resin drawn at different temperatures. The thermal properties for all drawing conditions of the 3D850 and 4043D resins are reported in Tables 5 and 6, respectively. Additionally, as an example, the thermograms of 3D850 filament drawn at a *FST* of 180 °C and of 4034D filament drawn at a *FST* of 160 °C are presented in Figure 6a,b, respectively.

Table 5. Thermal parameters of the drawn 3D850 filaments both before and after heat treatment.

Condition	T_g (°C)	T_m (°C)	X_c (%)
FST 170 °C	76.3 ± 0.2	175.5 ± 0.2	65.1 ± 0.4
FST 170 °C-HT	75.3 ± 0.2	175.1 ± 0.2	64.0 ± 0.3
FST 180 °C	76.4 ± 0.5	175.5 ± 0.2	62.9 ± 1.4
FST 180 °C-HT	75.1 ± 0.4	175.8 ± 0.2	62.7 ± 1.3

**Table 6.** Thermal parameters of the drawn 4043D filaments both before and after heat treatment.

Condition	T_g (°C)	T_{endo} * (°C)	T_m (°C)	X_c (%)
FST 140 °C	60.7 ± 0.5	-	149.4 ± 0.1	36.6 ± 0.5
FST 140 °C-HT	56.6 ± 0.2	127.3 ± 0.1	149.4 ± 0.1	37.9 ± 1.3
FST 150 °C	59.5 ± 0.1	-	149.6 ± 0.1	36.1 ± 0.1
FST 150 °C-HT	56.8 ± 0.7	127.2 ± 0.1	149.6 ± 0.1	38.0 ± 1.1
FST 160 °C	60.6 ± 0.7	-	149.7 ± 0.1	34.2 ± 0.1
FST 160 °C-HT	56.9 ± 0.1	127.0 ± 0.2	149.6 ± 0.2	36.9 ± 1.0

* Peak temperature of the first endothermic peak.

After heat treatment, all drawn fibers exhibited the glass transition at lower temperatures, indicating that the amorphous regions were more relaxed and molecules in this region found it easier to move. This result is consistent with the diameter increase and length reduction described in Section 3.1. It is worth noting that the 3D850 drawn fibers had no other significant changes in their thermal behavior, peak melting temperature, or crystallinity, as reported in Table 5 and shown in Figure 6a. On the other hand, 4043D-drawn filaments were affected by the heat treatment (Table 6 and Figure 6b). Not only did the crystallinity of all the fibers increase by about 2% after annealing, but a second endothermic peak also appeared at the beginning of the melting region. This peak has been attributed to the simultaneous α' to α transition that takes place during the DSC scan and the melt-recrystallization of the α-crystals formed during the previous heat treatment. The endothermic peak becomes sharper in the thermogram when the contribution of the second process is enhanced [6].

3.3. Mechanical Behavior

Typical stress–strain curves for the filaments before drawing (full lines) and after drawing (dashed lines) are presented in Figure 7. Black lines correspond to the untreated filaments, while grey lines correspond to the heat-treated ones. The undrawn filaments showed a defined yield point, followed by strain softening and a plateau until fracture occurred. The materials´ tensile behavior significantly changed upon drawing, showing strong strain hardening after yielding and much greater strains until sample fracture. Tensile parameter values relative to the corresponding values of the original filaments are listed in Table 7.
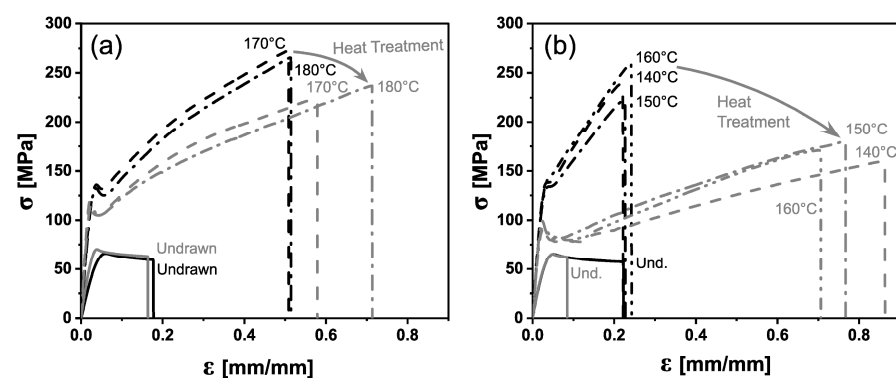
Figure 7. Typical stress (σ)- strain (ε) curves for the filaments before and after drawing at different *FST* (full and dotted lines, respectively) and before and after heat treatment (black and gray lines, respectively) for the (**a**) 3D850 and (**b**) 4043D resins.

Table 7. Mechanical properties of fibers drawn at different temperatures before (NT) and after heat-treating (HT) relative to corresponding values of original filaments.

Resin	Condition	Relative Tensile Apparent Modulus (%)		Relative Yield Strength (%)		Relative Stress at Break (%)		Relative Strain at Break (%)	
		NT	HT	NT	HT	NT	HT	NT	HT
3D850	Undrawn	0	68.3	0	7.3	0	10.9	0	−13.6
	FST 170 °C	236.0	286.2	103.4	72.1	364.6	284.6	186.4	277.4
	FST 180 °C	238.1	279.4	101.3	75.2	364.6	287.6	187.6	271.8
4043D	Undrawn	0	10.4	0	−0.46	0	7.8	0	−57.5
	FST 140 °C	176.0	134.7	106.9	36.1	309.9	174.6	12.4	340.9
	FST 150 °C	157.8	147.4	102.2	45.6	287.9	202.6	25.4	299.0
	FST 160 °C	176.9	132.3	112.2	42.6	356.8	187.9	27.5	269.4

Both 3D850 and 4043D filaments exhibited significant improvements in their mechanical properties after solid-state drawing. The material´s modulus for both resins significantly increased due to strain-induced crystallization; yield strength increased as a result of the restrictions to the molecular movement generated on the amorphous regions during drawing; and stress and strain at break were also greatly improved by the preferential orientation of the molecules in the drawing direction.

Drawing temperature showed no significant effects on the mechanical properties of the fibers obtained from the 3D850 resin. On the other hand, although the modulus and strain at break of the 4043D-drawn filaments displayed no statistically significant differences when drawn at different temperatures, an ANOVA analysis showed that the yield strength and stress at break of these filaments were affected by the applied draw ratio. It was pointed out in Section 3.1 that the draw ratio applied to the 4043D filaments depended on the drawing temperature. When the furnace was set at lower temperatures, heat transfer was more difficult and temperature distribution was less homogeneous on the fiber's section, resulting in hotter surfaces and colder cores. Therefore, the deformation of these filaments became more difficult. As revealed from morphological examinations, fibers drawn from 4043D resin presented a well-defined second opaque core at the center, which could be attributed to crazing or the formation of micro-voids during crystal formation caused by over-drawing [16,17].

It should also be noted that the mechanical properties of the solid-state drawn fibers obtained in this work are comparable to those of the commercial fibers studied in [22] (Yield strength = 102.4 (5.8) MPa; Stress at break = 258.3 (16.6) and Strain at break = 44.6 (4.1) %), being the ones of the 3D850 resin even slightly better in all studied properties.

The mechanical properties of the filaments after heat treatment are also summarized in Table 7. In 3D850 resin, which was specially designed to promote cold crystallization [9], annealing of the undrawn filament increased its crystallinity, therefore increasing the modulus. The presence of crystals also restricted molecular movement in the amorphous regions, causing a slight increase in the yield strength. On the other hand, 4043D resin was formulated to hinder cold crystallization and obtain transparent films [19]. Even though the undrawn filament became opaque and its dimensions changed after heat treatment, no significant variations were observed in their tensile parameters, indicating a limited effect of the cold crystallization in this case. However, a decrease in strain at break was promoted by annealing as a result of the already mentioned restriction imposed by crystals on the amorphous phase.

When drawn filaments of the 3D850 resin were heat treated, the material's tensile behavior remained unchanged (similar stress–strain curves), but there were significant variations in their mechanical properties (Figure 7a). Yield strength and stress at break decreased, and elongation at break increased due to the relaxation that took place during heat treatment, while modulus increased. Similar changes in stiffness have been reported in the literature for PLA filaments treated under taut conditions [16]. On the other hand, when

drawn fibers of the 4043D resin were annealed, their tensile behavior was severely affected (Figure 7b). Heat-treated fibers still exhibited strain hardening after yielding, but their yield strength and stress at break were much lower after heat treatment. They also displayed much more strain softening after yielding, and strain at break was greatly improved. Before annealing, there were no statistically significant differences in the modulus of fibers drawn at different temperatures, but after heat treatment, this was no longer valid. Samples drawn at a *FST* of 150 °C exhibited no statistically significant differences before and after heat treating, whereas the other two temperature conditions led to a slight modulus reduction on treated samples, which is consistent with the molecular relaxation induced by annealing. Even after drawing, 4043D filaments displayed comparatively lower crystallinity values than 3D850-drawn filaments or commercial fibers. Molecular orientation in the 4043D filaments could mostly occur upon drawing rather than crystal formation. As a result, significant shrinkage (about 30% of the original deformation) took place after treatment. This behavior has been attributed in the literature to locked-in stresses derived from stretched tie molecules spanning different crystallites [34].

It is worth noting that in all cases, even if any detrimental effect of heat treatment existed, the fibers obtained herein presented much better mechanical properties than the undrawn filaments.

4. Conclusions

In the present work, two commercial extruded filaments for 3D printing obtained from different NatureWorks PLA resins (different contents of D-isomer) were solid-state drawn and subsequently heat treated by annealing.

The thermal and mechanical properties obtained demonstrate that the drawing process used in this work is comparable to the processing techniques reported in the literature for PLA fiber production.

Heat treatment applied to drawn fibers has a completely different effect depending on the type of PLA resin. 3D850 fibers were much more stable than 4043D fibers after annealing since these fibers underwent molecular orientation upon drawing rather than crystallization, which was hindered by the higher content of D-ionomer in this resin.

Finally, it is worth noting that in all cases, even if any detrimental effect of heat treatment existed, the fibers obtained herein presented much better mechanical properties than the undrawn filaments, and these properties are in the same range as those of commercial fibers.

References

1. Lim, L.-T.; Auras, R.; Rubino, M. Processing technologies for poly(lactic acid). *Prog. Polym. Sci.* **2008**, *33*, 820–852. [CrossRef]
2. Henton, D.E.; Gruber, P.R.; Lunt, J.; Randall, J. Polylactic Acid Technology. In *Natural Fibers, Biopolymers, and Biocomposites*; Mohanty, A.K., Misra, M., Drzal, L.T., Eds.; CRC Press: Boca Raton, FL, USA, 2005; pp. 527–577.
3. Drumright, R.E.; Gruber, P.R.; Henton, D.E. Polylactic Acid Technology. *Adv. Mater.* **2000**, *12*, 1841–1846. [CrossRef]

4. Fischer, E.W.; Sterzel, H.J.; Wegner, G. Investigation of the structure of solution grown crystals of lactide copolymers by means of chemical reactions. *Kolloid-Z. Z. Polym.* **1973**, *251*, 980–990. [CrossRef]

5. Migliaresi, C.; Cohn, D.; De Lollis, A.; Fambri, L. Dynamic mechanical and calorimetric analysis of compression-molded PLLA of different molecular weights: Effect of thermal treatments. *J. Appl. Polym. Sci.* **1991**, *43*, 83–95. [CrossRef]

6. Pan, P.; Zhu, B.; Kai, W.; Dong, T.; Inoue, Y. Polymorphic Transition in Disordered Poly(l-lactide) Crystals Induced by Annealing at Elevated Temperatures. *Macromolecules* **2008**, *41*, 4296–4304. [CrossRef]

7. Persson, M.; Cho, S.-W.; Skrifvars, M. The effect of process variables on the properties of melt-spun poly (lactic acid) fibres for potential use as scaffold matrix materials. *J. Mater. Sci.* **2013**, *48*, 3055–3066. [CrossRef]

8. Pan, P.; Kai, W.; Hu, B.; Dong, T.; Inoue, Y. Polymorphous Crystallization and Multiple Melting Behavior of Poly(l-lactide): Molecular Weight Dependence. *Macromolecules* **2007**, *40*, 6898–6905. [CrossRef]

9. NatureWorks Ingeo Biopolymer 3D850 Technical Data Sheet: 3D Printing Monofilament—High Heat Grade. Available online: https://www.natureworksllc.com/~/media/Files/NatureWorks/Technical-Documents/Technical-Data-Sheets/TechnicalDataSheet_3D850_monofilament_pdf.pdf?la=en (accessed on 16 July 2023).

10. Gupta, B.; Revagade, N.; Hilborn, J. Poly(lactic acid) fiber: An overview. *Prog. Polym. Sci.* **2007**, *32*, 455–482. [CrossRef]

11. Sülar, V.; Oner, E.; Devrim, G.; Aslan, M.; Eser, B. A comparative study on performance properties of yarns and knitted fabrics made of biodegradable and conventional fibers. *Fibers Polym.* **2016**, *17*, 2085–2094. [CrossRef]

12. Mai, F.; Tu, W.; Bilotti, E.; Peijs, T. The Influence of Solid-State Drawing on Mechanical Properties and Hydrolytic Degradation of Melt-Spun Poly(Lactic Acid) (PLA) Tapes. *Fibers* **2015**, *3*, 523–538. [CrossRef]

13. Yang, Y.; Zhang, M.; Ju, Z.; Tam, P.Y.; Hua, T.; Younas, M.W.; Kamrul, H.; Hu, H. Poly(lactic acid) fibers, yarns and fabrics: Manufacturing, properties and applications. *Text. Res. J.* **2021**, *91*, 13–14. [CrossRef]

14. Kmetty, Á.; Bárány, T.; Karger-Kocsis, J. Self-reinforced polymeric materials: A review. *Prog. Polym. Sci.* **2010**, *35*, 1288–1310. [CrossRef]

15. Chui, Y.; Chuang, Y.; Kan, C. Effect of Heat Setting and Dyeing on Tensile Strength and Shrinkage Properties of Poly(Lactic Acid) Fibre. *Fibers Polym.* **2021**, *22*, 2388–2393. [CrossRef]

16. Cayuela, D.; Montero, L.; Riba, M.; Prieto, R.; Cano, F.; Manich, A.M. Relationship between microstructure and properties of false-twist textured and stabilized polylactide. Part 1: Dimensional stability, mechanical properties and thermomechanical behavior. *Text. Res. J.* **2013**, *83*, 1055–1064. [CrossRef]

17. Gao, C.; Ma, H.; Liu, X.; Yu, L.; Chen, L.; Liu, H.; Li, X.; Simon, G.P. Effects of thermal treatment on the microstructure and thermal and mechanical properties of poly(lactic acid) fibers. *Polym. Eng. Sci.* **2013**, *53*, 976–981. [CrossRef]

18. Dechet, M.A.; Demina, A.; Römling, L.; Gómez Bonilla, J.S.; Lanyi, F.J.; Schubert, D.W.; Bück, A.; Peukert, W.; Schmidt, J. Development of poly(L-lactide) (PLLA) microspheres precipitated from triacetin for application in powder bed fusion of polymers. *Addit. Manuf.* **2020**, *32*, 100966. [CrossRef]

19. NatureWorks IngeoTM Biopolymer 4043D Technical Data Sheet: 3D Printing Monofilament—General Purpose Grade. Available online: https://www.natureworksllc.com/~/media/Files/NatureWorks/Technical-Documents/Technical-Data-Sheets/TechnicalDataSheet_4043D_3D-monofilament_pdf.pdf?la=en (accessed on 16 July 2023).

20. Yazdaninia, A.; Khonakdar, H.A.; Jafari, S.H.; Asadi, V. Influence of trifluoropropyl-POSS nanoparticles on the microstructure, rheological, thermal and thermomechanical properties of PLA. *RSC Adv.* **2016**, *6*, 37149–37159. [CrossRef]

21. Backes, E.H.; Pires, L.N.; Costa, L.C.; Passador, F.R.; Pessan, L.A. Analysis of the Degradation During Melt Processing of PLA/Biosilicate®Composites. *J. Compos. Sci.* **2019**, *3*, 52. [CrossRef]

22. Bocz, K.; Domonkos, M.; Igricz, T.; Kmetty, Á.; Bárány, T.; Marosi, G. Flame retarded self-reinforced poly(lactic acid) composites of outstanding impact resistance. *Compos. Part A Appl. Sci. Manuf.* **2015**, *70*, 27–34. [CrossRef]

23. Walker, J.; Melaj, M.; Giménez, R.; Pérez, E.; Bernal, C. Solid-State Drawing of Commercial Poly(Lactic Acid) (PLA) Based Filaments. *Front. Mater.* **2019**, *6*, 280. [CrossRef]

24. Schippers, C.; Bahners, T.; Gutmann, J.; Tsarkova, L. Elaborating Mechanisms behind the Durability of Tough Polylactide Monofilaments under Elevated Temperature and Humidity Conditions. *ACS Appl. Polym. Mater.* **2021**, *3*, 1406–1414. [CrossRef]

25. Lim, L.-T.; Vanyo, J.; Randall, J.; Cink, K.; Agrawal, A.K. Processing of Poly(Lactic Acid). In *Poly(Lactic Acid): Synthesis, Structures, Properties, Processing, and Applications*, 2nd ed.; Auras, R.A., Lim, L.-T., Selke, S.E.M., Tsuji, H., Eds.; John Wiley & Sons, Inc.: Hoboken, UK, 2011; Part III; pp. 231–270.

26. *ISO 527-1:2019*; Plastics—Determination of Tensile Properties—Part 1: General Principles. International Organization for Standardization: Geneva, Switzerland, 2019.

27. Maspoch, M.L.; Santana, O.O.; Cailloux, J.; Franco-Urquiza, E.; Rodriguez, C.; Belzunce, J.; Martínez, A.B. Ductile-brittle transition behaviour of PLA/o-MMT films during the physical aging process. *Express Polym. Lett.* **2015**, *9*, 185–195. [CrossRef]

28. Tábi, T.; Sajó, I.E.; Szabó, F.; Luyt, A.S.; Kovács, J.G. Crystalline structure of annealed polylactic acid and its relation to processing. *Express Polym. Lett.* **2010**, *4*, 659–668. [CrossRef]

29. Cicero, J.A.; Dorgan, J.R. Physical Properties and Fiber Morphology of Poly(lactic acid) Obtained from Continuous Two-Step Melt Spinning. *J. Environ. Polym. Degr.* **2001**, *9*, 1–10. [CrossRef]

30. Liu, Y.; Yin, L.; Zhao, H.; Song, G.; Tang, F.; Wang, L.; Shao, H.; Zhang, Y. Lamellar and fibrillar structure evolution of poly(ethylene terephthalate) fiber in thermal annealing. *Polymer* **2016**, *105*, 157–166. [CrossRef]

31. Fambri, L.; Pegoretti, A.; Fenner, R.; Incardona, S.D.; Migliaresi, C. Biodegradable fibres of poly(l-lactic acid) produced by melt spinning. *Polymer* **1997**, *38*, 79–85. [CrossRef]

32. Kotsilkova, R.; Petrova-Doycheva, I.; Menseidov, D.; Ivanov, E.; Paddubskaya, A.; Kuzhir, P. Exploring thermal annealing and graphene-carbon nanotube additives to enhance crystallinity, thermal, electrical and tensile properties of aged poly(lactic) acid-based filament for 3D printing. *Compos. Sci. Technol.* **2019**, *181*, 107712. [CrossRef]

33. Gamez-Perez, J.; Velazquez-Infante, J.C.; Franco-Urquiza, E.; Pages, P.; Carrasco, F.; Santana, O.O.; Maspoch, M.L. Fracture behavior of quenched poly(lactic acid). *Express Polym. Lett.* **2011**, *5*, 82–91. [CrossRef]

34. Barham, P.; Keller, A. A criterion for distinguishing between polymer fibers of fundamentally different origin. *J. Polym. Sci. Polym. Lett. Ed.* **1975**, *13*, 197–202. [CrossRef]